

# Improved k-t BLAST and k-t SENSE using FOCUSS

**Hong Jung and Jong Chul Ye**‡

Bio-Imaging & Signal Processing Lab., Korea Advanced Institute of Science & Technology (KAIST), 373-1 Guseong-Dong, Yuseong-Gu, Daejeon 305-701, Republic of Korea

E-mail: [jong.ye@kaist.ac.kr](mailto:jong.ye@kaist.ac.kr)

**Eung Yeop Kim**

Yonsei University Medical Center, 134 Sinchon-dong, Seodaemun-gu, Seoul 120-752, Republic of Korea

**Abstract.** The dynamic MR imaging of time-varying objects, such as beating hearts or brain hemodynamics, requires a significant reduction of the data acquisition time without sacrificing spatial resolution. The classical approaches for this goal include parallel imaging, temporal filtering, and their combinations. Recently, model-based reconstruction methods called k-t BLAST and k-t SENSE have been proposed which largely overcome the drawbacks of the conventional dynamic imaging methods without *a priori* knowledge of the spectral support. Another recent approach called k-t SPARSE also does not require exact knowledge of the spectral support. However, unlike the k-t BLAST/SENSE, k-t SPARSE employs the so-called compressed sensing theory rather than using training. The main contribution of this paper is a new theory and algorithm that unifies the abovementioned approaches while overcoming their drawbacks. Specifically, we show that the celebrated k-t BLAST/SENSE are the special cases of our algorithm, which is asymptotically optimal from the compressed sensing theory perspective. Experimental results show that the new algorithm can successfully reconstruct a high resolution cardiac sequence and functional MRI data even from severely limited k-t samples, without incurring aliasing artifacts often observed in conventional methods.

‡ Corresponding Author. Email: [jong.ye@kaist.ac.kr](mailto:jong.ye@kaist.ac.kr).

## 1. Introduction

Dynamic MRI is a technique to monitor dynamic processes such as brain hemodynamics and cardiac motion. Fast imaging sequences, such as echo-planar imaging (EPI) [1] or balanced steady state free precession (bSSFP), have been widely used in practice for this purpose [2, 3]. EPI employs a series of bipolar readout gradients to generate a train of gradient echoes so that zigzag  $k$ -space trajectories can be sampled under the envelop of a free-induction decay (FID). Hence, EPI is commonly used for functional MR imaging. However, the use of EPI alone sacrifices the image quality to achieve high temporal resolution. The ultrafast sequence called balanced SSFP or TrueFISP is now a standard acquisition pulse sequence for cardiovascular MR due to its high blood signal-to-noise ratio (SNR) and blood-myocardium contrast-to-noise ratio (CNR) [3, 4]. However, for the left ventricular (LV) function study, 8-12 slices from the LV base to the apex with temporal resolution better than 60msec are often necessary [4]. Therefore, even with an ultrafast sequence, such as bSSFP or TrueFISP, the total volume acquisition within a single breath-hold is still challenging [4].

Parallel imaging methods can be used to improve the temporal resolution of a dynamic MRI. For example, SMASH (SiMultaneous Acquisition of Spatial Harmonics)[5], SENSE (SENSitivity Encoding) [6], PILS (Partially Parallel Imaging with Localized Sensitivities)[7], and GRAPPA (GeneRalized Autocalibrating Partially Parallel Acquisitions)[8] reduce the scan time by skipping the phase encoding steps. In the reconstruction phase, SENSE restores the original images from a set of aliased images by solving the linear sensitivity equation, whereas SMASH and GRAPPA calculate the missing  $k$ -space data directly using coil sensitivity to avoid aliasing. In principle, the data acquisition time for parallel imaging can be reduced up to the number of RF coils.

The method called UNFOLD (UNaliasing by Fourier-encoding the Overlaps Using the temporal Dimension)[9] is another method for fast data acquisition. More specifically, UNFOLD obtains the Fourier data in a  $k$ - $t$ -space in a sheared grid pattern, in which the phase encoding in  $k$ -space is shifted for every frame. This results in the repetition of the support region in  $x$ - $f$ -space, and the original image can be reconstructed using a spatio-temporal filter. Theoretically, the optimal UNFOLD design problem can be formulated as the spatio-temporal sampling problem in the  $k$ - $t$  space under the so-called time sequential sampling (TSS) constraint [10]. Willis and Bresler [11] showed that a high temporal and spatial resolution with a multifold reduction in the acquisition rate can be achieved using a lattice sampling schedule as long as the spectral supports are known.

Researchers have tried to combine UNFOLD with parallel imaging for even faster scanning or reduced artifacts. For example, TSENSE [12] combines UNFOLD with SENSE in such a way that any residual artifacts are temporally frequency-shifted to the band edge and thus may be further suppressed by temporal low-pass filtering; whereas UNFOLD-SMASH [13] obtains the additional phase encoding lines using SMASH, after which images are reconstructed using UNFOLD. A generalization of the optimized time sequential sampling theory by Willis and Bresler [11] for the phase array coil data acquisition has recently been

independently proposed by Sharif et al [14] and Kim et al [15]. The noticeable difference of the new methods from [11] is that these methods allow aliasing in the x-f domain in designing a sampling lattice. The aliased x-f image is then converted into the final aliasing free x-f image by exploiting the coil sensitivities. In theory, the maximal achievable acceleration factor can be up to the parallel imaging acceleration factor multiplied by that of the optimized time sequential sampling. However, the main technical difficulties of these algorithms are that 1) the x-f supports are not usually band-limited and that 2) the exact knowledge of the x-f supports are difficult to obtain.

Recently, model based approaches called *k-t* BLAST and *k-t* SENSE have been proposed which largely overcome the shortcomings of the existing algorithms [16, 17, 18, 19]. The *k-t* BLAST and *k-t* SENSE take advantage of *a priori* information about the x-f support obtained from the training data set in order to enhance the image resolution during data acquisition time. Unlike the other methods, *k-t* BLAST and *k-t* SENSE do not require precise knowledge of the spectral support. Furthermore, the signal does not need finite support. Even if the spectral supports overlap due to aliasing, *a priori* information from the training data can be used to remedy the aliasing artifacts. Significant quality improvements have been reported compared to the conventional methods. Furthermore, using regular lattice sampling patterns, fast implementation is possible.

Other interesting dynamic MR imaging approaches are closely related to the recent theory of the “compressed sensing” in the signal processing community [20, 21], for example, *k-t* SPARSE [22]. According to the compressed sensing theory, perfect reconstruction is possible, even from samples dramatically smaller than the Nyquist sampling limit, as long as the non-zero spectral support is sparse and the samples are obtained at random locations [20]. Even if the signal is not sparse, we can still recover the significant features of the signals if the signals are compressible. Furthermore, optimal sparse solutions can be obtained using computationally feasible  $L_1$  minimization algorithms, such as the basis pursuit, matching pursuit methods, etc., rather than resorting to computationally expensive combinatorial optimization algorithms [20, 21]. Hence, the compressed sensing theory has great potential to solve imaging problems. The *k-t* SPARSE successfully employed the compressed sensing theory for cardiac imaging applications by transforming the time varying image using a wavelet transform along the spatial direction and the Fourier transform along the temporal direction [22]. The compressed sensing idea has been also used for the MR angiography problem as well [23]. However, the main drawback of *k-t* SPARSE is the computational burden. Furthermore, due to the total variational regularization used in [22, 23], cartoon-like artifacts are often observed. Related regularization based algorithms have been also presented to reduce the temporal aliasing artifacts using regularization techniques [24].

One of the main contributions of this paper is the new algorithm called *k-t* FOCUSS (*k-t* space FOCal Underdetermined System Solver (FOCUSS)) that unifies the abovementioned approaches while overcoming their drawbacks. We show that our *k-t* FOCUSS is asymptotically optimal from a compressed sensing perspective and the celebrated *k-t* BLAST

and *k-t* SENSE are the special cases of *k-t* FOCUSS.

The basis of *k-t* FOCUSS is another important class of sparse reconstruction algorithm called the FOCal Underdetermined System Solver (FOCUSS) [25, 26, 27]. FOCUSS was originally designed to obtain sparse solutions by successively solving quadratic optimization problems and has been successfully used for EEG source localization [25, 26]. More specifically, FOCUSS starts by finding a low resolution estimate of a sparse signal, and then this solution is pruned to a sparse signal representation. The pruning process is implemented by scaling the entries of the current solution by those of the solutions of previous iterations. Hence, once some entries of the previous solution become zero, these entries are fixed to zero values. As a consequence, we can obtain a sparser solution with more iterations. During the pruning process, the entries corresponding to the zero values on the original spectral support converge to zero. Hence, one of the important requirements of FOCUSS is the existence of a reasonable low-resolution initial estimate which provides the necessary extra constraint to resolve the non-uniqueness of the problem.

FOCUSS is a nice fit to the dynamic MRI. First, the training data or interleaved low frequency *k-t* samples can provide the low-resolution initial estimate essential for the convergence of FOCUSS. Second, FOCUSS incorporates the sparseness as a soft-constraint, whereas the conventional basis pursuit or orthogonal matching pursuit impose the constraint as a hard-constraint. The hard sparseness constraint may be not suitable for dynamic MRI since the abrupt changes of the image values introduce visually annoying high frequency artifacts as reported in *k-t* SPARSE, especially when combined with total variation regularization [22]. The reconstruction image using FOCUSS, however, does not exhibit these behaviors since the non-zero image values are gradually suppressed. Third, FOCUSS can be very easily implemented in a computationally efficient manner using successive quadratic optimization. This is quite a big advantage over the other sparse optimization algorithms, such as basis pursuit or matching pursuit approaches. Finally, FOCUSS asymptotically achieves the optimal solution from the compressed sensing theory point of view. Experimental results demonstrate very quick convergence of the *k-t* FOCUSS to accurate solutions, even from highly sparse *k*-space samples.

This paper is organized as follows. Section 2 provides a detailed discussion of *k-t* FOCUSS. In Section 3, the implementation issues of *k-t* FOCUSS are discussed. Our experimental results and discussion are presented in Sections 4 and 5, respectively. Conclusions are given in Section 6.

## 2. Theory

### 2.1. Problem Formulation

Consider the cartesian trajectory. The readout direction is along the  $k_y$  axis, and  $k_x$  denotes the phase encoding direction. The samples along the readout direction are fully sampled within  $T_R$ . Let  $\sigma(x, t)$  denote the unknown image content (for example, proton density,

T1/T2 weighted image, etc.) on  $x$  at time instance  $t$ . Then, the  $k$ -space measurement  $v(k, t)$  at time  $t$  is given by

$$v(k, t) = \int \sigma(x, t) e^{-j2\pi kx} dx = \int \int \rho(x, f) e^{-j2\pi(kx+ft)} dx df, \quad (1)$$

where  $\rho(x, f)$  denotes the 2-D spectral support in the  $x$ - $f$  domain, and we use the following Fourier transform along the temporal direction:

$$\sigma(x, t) = \int \rho(x, f) e^{-j2\pi ft} df. \quad (2)$$

Let  $\rho[n_x, n_f]$  denote the discretized  $(x, f)$ -image on  $x = n_x \Delta x, n_x = 1, 2, \dots, N_x$  and  $f = n_f \Delta f, n_f = 1, 2, \dots, N_f$ , where  $\Delta x$  and  $\Delta f$  denote the sampling steps for  $x$  and  $f$ , respectively. Then, the  $k$ -space measurement  $v[n_k, n_t]$  at the  $k$ -space location  $k = n_k \Delta k, n_k = 1, \dots, N_k$  and the time instance  $t = n_t \Delta t, n_t = 1, \dots, N_t$  can be approximated by the 2-D discrete Fourier transform:

$$v[n_k, n_t] = \Delta x \Delta f \sum_{n_x=1}^{N_x} \sum_{n_f=1}^{N_f} \rho[n_x, n_f] e^{-j2\pi(n_k n_x \Delta k \Delta x + n_f n_t \Delta f \Delta t)}. \quad (3)$$

According to the Nyquist sampling limit theory, to obtain an aliasing free image, the interval  $\Delta k$  on  $k$ -space should be  $\Delta k \leq 1/(N_x \Delta x)$ . In the same way, to reconstruct a time varying image without temporal aliasing, we need  $\Delta t \leq 1/(N_f \Delta f)$ . Hence, at the Nyquist sampling rate, we have

$$v[n_k, n_t] = \frac{1}{\Delta k \Delta t N_x N_f} \sum_{n_x=1}^{N_x} \sum_{n_f=1}^{N_f} \rho[n_x, n_f] e^{-j2\pi(n_k n_x / N_x + n_f n_t / N_f)}. \quad (4)$$

In matrix form, Eq. (4) can be represented by

$$\mathbf{v} = \mathbf{F} \boldsymbol{\rho}, \quad (5)$$

where  $\mathbf{v}$  and  $\boldsymbol{\rho}$  denote the stacked  $k$ - $t$  space measurement vectors and the  $x$ - $f$  image, respectively, and  $\mathbf{F}$  denotes the 2-D Fourier transform along  $x$ - $f$  direction. Here, it is important to note that the temporal Fourier transform Eq. (2) corresponds to a sparsifying operator of periodic motions, such as cardiac motion since the corresponding spectrum is the line spectrum from the Fourier series rather than the continuous spectrum. For general motions, there may exist more efficient transform to sparsify the signal, which will be discussed later.

Our main goal is to reduce the number of samples in the  $k$ - $t$  space without sacrificing  $x$ - $f$  image quality by taking advantage of the sparsity of  $x$ - $f$  support. Here, recent theory of the compressed sensing (CS) [20, 21, 28, 29, 30] can be applied. The compressed sensing theory tells us that the *perfect* reconstruction of  $\boldsymbol{\rho}$  is possible from the *noiseless*  $k$ - $t$  space samples that are dramatically smaller than the Nyquist sampling limit as long as the non-zero support

of  $\boldsymbol{\rho}$  is sparse and the *k-t* samples are obtained at random. More specifically, if  $\boldsymbol{\rho}$  is nonzero at the *unknown*  $M$  locations, then the number of required *k-t* space measurement,  $K$ , can be dramatically smaller than the *x-f* domain pixel number,  $N = N_x N_f$ , and it is possible to design  $K = O(M \log(N))$  number of measurements to obtain the perfect reconstruction of  $\boldsymbol{\rho}$  with overwhelming probability by solving a  $L_1$  minimization problem<sup>§</sup>. Second, if  $K = O(M \log^6(N))$  discrete measurements in *k-t* space are *noisy* and their magnitudes are upper-bounded by the input noise power  $\epsilon$ , then with overwhelming probability the reconstruction error is still upper bounded by  $\epsilon$  multiplied with a finite constant. This concept can be effectively applied to dynamic MR imaging since only limited frequency components have significant values on *x-f* support of a dynamic sequence. Hence, we can expect the *graceful degradation* of the reconstruction image quality if the compressed sensing approach is applied for dynamic MR imaging problems.

Perhaps the most important implication of the compressed sensing theory is that the optimal sparse solution satisfying the abovementioned properties can be obtained by solving the  $L_1$  minimization [20, 21]. More specifically, the optimal dynamic MR imaging problem from the compressed sensing perspective can be stated as follows:

$$\begin{aligned} & \text{minimize } \|\boldsymbol{\rho}\|_1 \\ & \text{subject to } \|\mathbf{v} - \mathbf{F}\boldsymbol{\rho}\|_2 \leq \epsilon \end{aligned} \quad (6)$$

where  $\|\cdot\|_1$  and  $\|\cdot\|_2$  denote the  $L_1$  and  $L_2$  norm, respectively, and  $\epsilon$  denotes the noise level.

## 2.2. Derivation of *k-t* FOCUSS

As explained before, the idea of compressed sensing is not new in the MR community. The *k-t* SPARSE [22] successfully employed the compressed sensing theory for cardiac imaging applications by transforming the time varying image using a wavelet transform along the spatial direction and the Fourier transform along the temporal direction. However, our compressed sensing approach is very different from [22] and is much closer to *k-t* BLAST and *k-t* SENSE. This is because the basis of our approach is another type of sparse reconstruction method called the FOCal Underdetermined System Solver (FOCUSS) [25, 26, 27].

FOCUSS is an algorithm designed to obtain the sparse solutions to the underdetermined linear inverse problem given by [26, 27]

$$\mathbf{v} = \mathbf{F}\boldsymbol{\rho} . \quad (7)$$

The solution of Eq. (7) is not unique; hence, the minimum norm solution is the most widely accepted. The minimum solution, however, does not provide a sparse reconstruction and has the tendency to smooth out the energy [26, 27]. Now, let us consider the following optimization problem:

$$\text{find } \boldsymbol{\rho} = \mathbf{W}\mathbf{q} \quad (8)$$

<sup>§</sup> The  $O(\cdot)$  denotes the ‘‘big O’’ notation to describe an asymptotic upper bound.

where  $\boldsymbol{\rho}$  is an unknown x-f support,  $\mathbf{W}$  is a weighting matrix, and  $\mathbf{q}$  is a solution of the following constrained minimization problem:

$$\min \|\mathbf{q}\|_2, \quad \text{subject to } \|\mathbf{v} - \mathbf{FW}\mathbf{q}\|_2 \leq \epsilon. \quad (9)$$

The constrained optimization problem can be converted into the un-constrained optimization problem using the Lagrangian multiplier, providing a cost function:

$$C(\mathbf{q}) = \|\mathbf{v} - \mathbf{FW}\mathbf{q}\|_2^2 + \lambda \|\mathbf{q}\|_2^2 \quad (10)$$

where  $\lambda$  denotes the appropriate Lagrangian parameter. The optimal solution minimizing Eq. (10) is then given by

$$\begin{aligned} \boldsymbol{\rho} &= \mathbf{W}\mathbf{q} \\ &= \boldsymbol{\Theta}\mathbf{F}^H (\mathbf{F}\boldsymbol{\Theta}\mathbf{F}^H + \lambda\mathbf{I})^{-1} \mathbf{v} \end{aligned} \quad (11)$$

where  $\boldsymbol{\Theta} = \mathbf{W}\mathbf{W}^H$ . In a slightly different formulation,  $\boldsymbol{\rho}$  is initialized with non-zero values  $\bar{\boldsymbol{\rho}}$ . In this case, the cost function Eq. (10) can be modified into the following form:

$$C(\mathbf{q}) = \|\mathbf{v} - \mathbf{F}\bar{\boldsymbol{\rho}} - \mathbf{FW}\mathbf{q}\|_2^2 + \lambda \|\mathbf{q}\|_2^2 \quad (12)$$

where  $\boldsymbol{\rho} = \bar{\boldsymbol{\rho}} + \mathbf{W}\mathbf{q}$ , and the optimal solution is then given by

$$\boldsymbol{\rho} = \bar{\boldsymbol{\rho}} + \boldsymbol{\Theta}\mathbf{F}^H (\mathbf{F}\boldsymbol{\Theta}\mathbf{F}^H + \lambda\mathbf{I})^{-1} (\mathbf{v} - \mathbf{F}\bar{\boldsymbol{\rho}}). \quad (13)$$

The novelty of FOCUSS algorithm comes from the fact that the weighting matrix  $\mathbf{W}$  can be continuously updated using the previous solution (hence,  $\boldsymbol{\Theta} = \mathbf{W}\mathbf{W}^H$  is updated accordingly). More specifically, if the  $(n-1)$ -th iteration of the image estimate is given by

$$\boldsymbol{\rho}_{n-1} = [\rho_{n-1}(1), \rho_{n-1}(2), \dots, \rho_{n-1}(N)]^T, \quad (14)$$

where  $N$  is the total number of data on x-f space, then the  $n$ -th iteration of FOCUSS can be calculated by the following procedure [27]:

(i) Compute the weighting matrix  $\mathbf{W}_n$ :

$$\mathbf{W}_n = \begin{pmatrix} |\rho_{n-1}(1)|^p & 0 & \cdots & 0 \\ 0 & |\rho_{n-1}(2)|^p & \cdots & 0 \\ \vdots & \vdots & \ddots & \vdots \\ 0 & 0 & \cdots & |\rho_{n-1}(N)|^p \end{pmatrix}, \quad 1/2 \leq p \leq 1. \quad (15)$$

(ii) Compute  $\boldsymbol{\Theta}_n = \mathbf{W}_n\mathbf{W}_n^H$ .

(iii) Compute the  $n$ -th FOCUSS estimate:

$$\boldsymbol{\rho}_n = \boldsymbol{\Theta}_n\mathbf{F}^H (\mathbf{F}\boldsymbol{\Theta}_n\mathbf{F}^H + \lambda\mathbf{I})^{-1} \mathbf{v}. \quad (16)$$

or, in another form:

$$\boldsymbol{\rho}_n = \bar{\boldsymbol{\rho}} + \boldsymbol{\Theta}_n\mathbf{F}^H (\mathbf{F}\boldsymbol{\Theta}_n\mathbf{F}^H + \lambda\mathbf{I})^{-1} (\mathbf{v} - \mathbf{F}\bar{\boldsymbol{\rho}}). \quad (17)$$

(iv) If it converges, stop. Otherwise, increase  $n$  and go to Step 1.

In order to understand why FOCUSS can provide a sparse solution, consider the  $n$ -th FOCUSS estimate of the weighting matrix,  $\mathbf{W}_n$ . Then, Eqs. (8) and (9) can be equivalently represented by

$$\min \|\mathbf{W}_n^{-1} \boldsymbol{\rho}\|_2^2, \quad \text{subject to } \|\mathbf{v} - \mathbf{F}\boldsymbol{\rho}\|_2 \leq \epsilon \quad (18)$$

Now we set  $p = 0.5$  for Eq. (15). Then, we have the following asymptotic relation:

$$\begin{aligned} \|\mathbf{W}_n^{-1} \boldsymbol{\rho}\|_2^2 &= \boldsymbol{\rho}^H \mathbf{W}_n^{-H} \mathbf{W}_n^{-1} \boldsymbol{\rho} \\ &= \boldsymbol{\rho}^H \begin{pmatrix} |\rho_{n-1}(1)|^{-1} & 0 & \cdots & 0 \\ 0 & |\rho_{n-1}(2)|^{-1} & \cdots & 0 \\ \vdots & \vdots & \ddots & \vdots \\ 0 & 0 & \cdots & |\rho_{n-1}(N)|^{-1} \end{pmatrix} \boldsymbol{\rho} \\ &\sim \sum_{i=1}^N |\rho_{n-1}(i)| \quad \text{as } n \rightarrow \infty \\ &= \|\boldsymbol{\rho}\|_1 \end{aligned} \quad (19)$$

where  $\sim$  implies the asymptotic equality as  $n \rightarrow \infty$ . This implies that the FOCUSS solution is asymptotically equivalent to the  $L_1$  minimization solution when  $p$  is set to 0.5. At this time,  $L_1$  is defined as the sum of the absolute values of the whole data. Since the  $L_1$  minimization is the preferred optimization method for compressed sensing [20], the FOCUSS solution will asymptotically converge to the optimal solution from compressed sensing perspective by setting  $p = 0.5$ . Furthermore, according to [26], for  $0.5 \leq p < 1$ , the FOCUSS provides sparse solutions.

In summary, FOCUSS starts by finding a low resolution estimate of the  $\rho(x, f)$  to initialize the  $\mathbf{W}_n$  matrix at  $n = 0$ , and this solution is *pruned* to a sparse signal representation. The pruning process is implemented by scaling the entries of the current solution by those of the solutions of previous iterations [26]. Therefore, a good initial estimate of  $\rho(x, f)$  is an important factor to guarantee the performance of the algorithm. In our implementation of  $k$ -t FOCUSS for dynamic MRI, we employ the random sampling pattern with more samples around low frequency region. Hence, the initial estimate can be easily obtained from the zero-padded direct Fourier inversion result without additional training data. Of course, an additional training set could be also used for the initial estimate of  $\mathbf{W}_0$ .

Recall that the  $k$ -t BLAST algorithm is given by [16]

$$\boldsymbol{\rho}_1 = \bar{\boldsymbol{\rho}} + \boldsymbol{\Theta}_0 \mathbf{F}^H (\mathbf{F} \boldsymbol{\Theta}_0 \mathbf{F}^H + \lambda \mathbf{I})^{-1} (\mathbf{v} - \mathbf{F} \bar{\boldsymbol{\rho}}) \quad (20)$$

where  $\boldsymbol{\Theta}_0$  is the diagonal covariance matrix obtained from the training data set and  $\bar{\boldsymbol{\rho}}$  corresponds to the DC component (i.e.  $f = 0$ ) in the  $x$ - $f$  image. Comparing Eq. (20) with Eq. (17), we find that the conventional  $k$ -t BLAST is indeed the first iteration of our  $k$ -t FOCUSS algorithm when the  $p$  value of Eq. (15) is set to 1 and the  $\bar{\boldsymbol{\rho}}$  is initialized using

the temporal average (DC) values. Other advantages of our algorithm over k-t BLAST are summarized as follows:

- (i) Our k-t FOCUSS is asymptotically optimal from the compressed sensing perspective. However, k-t BLAST does not minimize the  $L_1$  norm, hence it is not optimal from the compressed sensing perspective.
- (ii) Instead of using  $p = 1$  value for the diagonal matrix  $\Theta_0$  as in k-t BLAST, our k-t FOCUSS can choose any values between 0.5 and 1. It turns out that  $p = 0.5$  is usually the best choice that guarantees the stability and improved reconstruction quality.

### 2.3. k-t FOCUSS for Parallel Imaging

The extension of k-t FOCUSS to parallel imaging is quite straightforward. Recall that the measurement from a parallel coil is given by the 2-D Fourier relationship:

$$v[n_k, n_t] = \frac{1}{\Delta k \Delta t N_x N_f} \sum_{n_x=1}^{N_x} \sum_{n_f=1}^{N_f} s_i[n_x] \rho[n_x, n_f] e^{-j2\pi(n_k n_x / N_x + n_f n_t / N_f)} \quad i = 1, \dots, N_c \quad (21)$$

where  $s_i[n_x]$  denotes the  $i$ -th coil sensitivity at  $x = n_x \Delta x$  and  $N_c$  is the number of coils. In matrix form, Eq. (21) can be represented by

$$\mathbf{v}_i = \mathbf{F} \mathbf{S}_i \boldsymbol{\rho} \quad (22)$$

where  $\mathbf{S}_i$  denotes the diagonal matrix composed of the  $i$ -th sensitivity  $s_i[n_x]$ . Then, the cost function of the  $n$ -th FOCUSS iteration becomes

$$C(\mathbf{q}) = \left\| \hat{\mathbf{v}} - \hat{\mathbf{F}} \mathbf{W}_n \mathbf{q} \right\|_2^2 + \lambda \|\mathbf{q}\|_2^2 \quad (23)$$

where  $\hat{\mathbf{F}}$  and  $\hat{\mathbf{v}}$  are given by

$$\hat{\mathbf{v}} = \begin{bmatrix} \mathbf{v}_1 \\ \vdots \\ \mathbf{v}_{N_c} \end{bmatrix}, \hat{\mathbf{F}} = \begin{bmatrix} \mathbf{F} \mathbf{S}_1 \\ \vdots \\ \mathbf{F} \mathbf{S}_{N_c} \end{bmatrix}. \quad (24)$$

Then, the optimal  $n$ -th k-t FOCUSS update is given by

$$\boldsymbol{\rho}_n = \Theta_n \hat{\mathbf{F}}^H \left( \hat{\mathbf{F}} \Theta_n \hat{\mathbf{F}}^H + \lambda \mathbf{I} \right)^{-1} \hat{\mathbf{v}} \quad (25)$$

where  $\Theta_n = \mathbf{W}_n \mathbf{W}_n^H$ . Furthermore, if we initialize  $\boldsymbol{\rho}$  with  $\bar{\boldsymbol{\rho}}$ , we have

$$\boldsymbol{\rho}_n = \bar{\boldsymbol{\rho}} + \Theta_n \hat{\mathbf{F}}^H \left( \hat{\mathbf{F}} \Theta_n \hat{\mathbf{F}}^H + \lambda \mathbf{I} \right)^{-1} \left( \hat{\mathbf{v}} - \hat{\mathbf{F}} \bar{\boldsymbol{\rho}} \right) \quad (26)$$

Again, the first iteration of Eq. (26) corresponds to k-t SENSE.

A slightly different, but computationally more efficient implementation of the k-t FOCUSS for parallel imaging can be obtained by separately applying k-t FOCUSS for each coil. More specifically, the algorithm is given by

- (i) For each coil measurements  $\mathbf{v}_i$ , apply the *k-t* FOCUSS to obtain the  $i$ -th estimate  $\hat{\mathbf{y}}_i = \mathbf{S}_i \hat{\boldsymbol{\rho}}$ , where  $i = 1, \dots, N_c$ .
- (ii) From  $\hat{\mathbf{y}}_i, i = 1, \dots, N_c$ , find the least square estimate  $\hat{\boldsymbol{\rho}}$ :

$$\hat{\boldsymbol{\rho}} = \left( \sum_{i=1}^{N_c} \mathbf{S}_i \mathbf{S}_i^H \right)^{-1} \left( \sum_{i=1}^{N_c} \mathbf{S}_i^H \hat{\mathbf{y}}_i \right) \quad (27)$$

#### 2.4. *k-t* FOCUSS using KLT/PCA

Even though our *k-t* FOCUSS has been developed using the temporal Fourier transform given in Eq. (2), a more general transform could be employed. The temporal Fourier transform is effective in sparsifying the signal when the image follows the periodic motion. However, for the objects with more general motion, other transforms may be more efficient in sparsifying the signal.

In the image and signal processing literature, an important transform for data compression is the Karhunen-Loeve transform (KLT), or the Principle Component Analysis (PCA) [31]. Unlike the Fourier transform, the KLT/PCA is a data dependent transform. More specifically, let  $\boldsymbol{\sigma}_x$  denote the discretized time varying proton density at  $x$  as follows:

$$\boldsymbol{\sigma}_x = \left[ \sigma(x, \Delta t) \quad \sigma(x, 2\Delta t) \quad \dots \quad \sigma(x, N_t \Delta t) \right]^T \in \mathbf{C}^{N_t} \quad (28)$$

Then, the covariance matrix  $\mathbf{C}_x$  of  $\boldsymbol{\sigma}_x$  can be expanded as follows:

$$\mathbf{C}_x = \sum_{k=1}^{N_t} \lambda_k \boldsymbol{\psi}_k \boldsymbol{\psi}_k^H \quad (29)$$

where  $\{\lambda_k\}_{k=1}^{N_t}$  and  $\{\boldsymbol{\psi}_k\}_{k=1}^{N_t}$  are the eigenvalues and the corresponding orthonormal eigenvectors (or principle components) of  $\mathbf{C}_x$  [31]. Using Eq. (29), we can create the following expansion [31]:

$$\boldsymbol{\sigma}_x = \sum_{k=1}^{N_t} \rho_k^x \boldsymbol{\psi}_k \quad (30)$$

for some expansion coefficients  $\boldsymbol{\rho}^x = \{\rho_k^x\}_{k=1}^{N_t}$ . It is well-known that the KLT/PCA is the optimal energy compaction transform and that most of the energy is compacted in a small number of expansion coefficients [31], which is an ideal property from the compressed sensing perspective.

Note that the principle components  $\{\boldsymbol{\psi}_k\}_{k=1}^{N_t}$  in Eq. (30) are data dependent, hence they are, in fact, varying with respect to the specific  $x$  position. However, estimating autocovariance for each  $x$  position is a very underdetermined problem due to the limited number of measurements. Hence, assuming that the motion of the moving parts are about the same for all  $x$  position, we can estimate the autocovariance function using measurements from all  $x$ 's. More specifically, in our *k-t* FOCUSS implementation, the low resolution initial

image can be easily obtained from training or interleaved low frequency *k*-space samples. This information is used to estimate the covariance matrix  $\mathbf{C}_x$ . Then, the principle component  $\{\boldsymbol{\psi}_k\}_{k=1}^{N_t}$  can be readily obtained using eigen-decomposition. It is important to note that even though principal components are obtained from low spatial resolution images, the temporal changes are not smoothed at all because we use fully sampled data along temporal direction within limited low spatial frequency *k*-space in order to obtain full set of principal components. Therefore, the KLT/PCA keeps any high temporal frequency information.

After obtaining the expansion Eq. (30), the remaining part of our *k-t* FOCUSS algorithm is exactly the same as the temporal Fourier transform. More specifically, the unknown image vector to reconstruct is the KLT coefficients given by

$$\boldsymbol{\rho} = \left[ \boldsymbol{\rho}^{\Delta x} \quad \boldsymbol{\rho}^{2\Delta x} \quad \dots \quad \boldsymbol{\rho}^{N_x \Delta x} \right]^T \in \mathbb{C}^{N_x N_t \times 1}. \quad (31)$$

and the mapping  $\mathbf{F}$  of Eq. (7) is given by the composite mapping of 1-D DFT matrix with the eigenvector basis from KLT/PCA. Hence, we will not elaborate on the details of the implementation to avoid any duplicated explanation. In Section 4, we will show that the KL transform is very effective for functional MRI analysis.

### 3. Implementation Issues

In [19], the influence of the training set quality in the *k-t* BLAST was discussed in detail. The key observation was that the training set needs not produce a high resolution covariance matrix estimate, and a low resolution estimate is sufficient. Such observations in [19] can be easily explained from a FOCUSS point of view. Our previous analysis showed that  $\Theta$  in the *k-t* BLAST comes from the reweighted norm concept in the FOCUSS rather than the covariance matrix. Since FOCUSS is a pruning algorithm that prunes a low resolution image to a sparse image by reweighting the image using the previous reconstruction results, we do not need a high resolution initial estimate of a *x-f* image.

Figure 1 illustrates an example of the *k-t* sampling pattern used in our paper. We generated samples according to a random distribution since the basic assumption of the compressed sensing is the use of a random sampling pattern. In order to obtain a low resolution initial estimate without an additional training phase, a zero mean Gaussian distribution is used to generate a random sampling pattern with more frequent *k*-space samples at the spatial low frequency regions.

The whole flow chart of our *k-t* FOCUSS algorithm is illustrated in Figure 2. Here, the temporal average contribution is first subtracted from *k-t* samples, which are then converted to the *x-f* domain using the Fourier transform. The weighting matrix  $\mathbf{W}$  at the first iteration is then obtained from the low resolution initial estimate of *x-f* support using Eq. (15). In principle, any power factor between  $0.5 \leq p \leq 1$  could be used for Eq. (15). However, extensive simulation shows that the solution for  $p = 1$  is too sparse, and  $p < 0.5$  does not effectively remove the aliasing pattern from the random sampling pattern. Hence, the

choice of  $p = 0.5$  seems to be optimal in many applications. After the weighting matrix is constructed, a FOCUSS iteration step is performed. The newly calculated FOCUSS estimate of x-f support is then again used to recalculate the  $\mathbf{W}$  matrix. These steps are successively applied to obtain consecutive k-t FOCUSS estimates.

As discussed in the previous section, the KL transform can be used as a sparsifying transform. In this case, Figure 2 should be changed accordingly to reflect that the  $\rho$  is no longer in the x-f domain. However, all the remaining reconstruction flowchart is exactly the same.

## 4. Experimental Results

### 4.1. In Vivo Cardiac Cine Imaging

*4.1.1. Methods* For *in vivo* experiments, we have acquired 25 frames of full k-space data from a cardiac cine of a patient using a 1.5 T Philips scanner at Yonsei University Medical Center. The field of view (FOV) was  $345.00 \times 270.00 \text{mm}^2$ , and the matrix size for scanning was  $256 \times 220$ , which corresponds to 220 phase encoding steps and 256 samples in frequency encoding. In these experiments, the phase encodings direction is horizontal. The slice thickness was 10.0 mm, and the acquisition sequence was steady-state free precession (SSFP) with a flip angle of 50 degree and  $T_R = 3.45 \text{msec}$ . The heart frequency was 66 bpm, and the retrospective cardiac gating was used. The magnitude image of this reconstructed *complex valued* cardiac cine from the full k-space samples is used as a ground-truth reference image to evaluate the reconstruction quality of k-t FOCUSS.

In the first simulation, we extracted 55 phase encodings from the full 220 phase encodings using the Gaussian random sampling pattern, which corresponds to the reduction factor of four. Since the downsampling was done using *actual* k-space measurement data, no Hermitian symmetry was assumed. This allows us to evaluate the effects of phase variations during the MR acquisition. Additionally, we have tested our k-t FOCUSS algorithm from a higher reduction factor like 8x or 16x acceleration. Also, for these higher reduction factors, we apply parallel imaging version of k-t FOCUSS to improve the results.

*4.1.2. Results* We have analyzed the reconstruction performance of k-t FOCUSS with iterations. Since the downsampling is along the phase encoding direction, the aliasing patterns along horizontal direction were observed when the cardiac cine was reconstructed using the zero-padded Fourier transform (see Figure 3(b)). When our k-t FOCUSS algorithm is applied to these images, more iterations significantly improve the image quality, but after the fifth iteration, little improvement was observed, indicating that k-t FOCUSS has converged (see Figures 4(c)-(d)). We have also illustrated the corresponding x-f supports in the right column of Figures 3 and 4. The original x-f support is sparse. The estimated x-f support for the fifth iteration of k-t FOCUSS is sparse and clearly catches the significant part of the true x-f support. Additionally, we have also illustrated reconstruction results using

the sliding window method with the window size of four in Figure 4(a). The sliding window method was implemented as follows. First, to fill out the missing *k*-space samples for each frame, the *k*-space data in neighboring frames were used. The window was centered on the current frame, and the nearest *k*-data from the current frame within the window were used to fill out the missing *k*-space samples on the current frame. After applying this procedure for every frame, we were able to reconstruct the time varying image sequences. As shown in Figure 4, our *k-t* FOCUSS results outperform it.

In order to show the difference clearly, we have calculated the difference images between the original cardiac cine and the reconstruction results from the down sampled data. Figure 5(a) shows the difference images between the original and reconstructed images from the sliding window methods using the window size four. The aliasing artifacts along phase encoding direction are observed. Figure 5 (b) shows the difference images between the original and the first iteration of *k-t* FOCUSS. Here, the artifacts are still strong along phase encoding direction. We can also observe that the artifacts at the cardiac boundary are significant due to temporal blurring. However, at the fifth iteration of *k-t* FOCUSS, as shown in Figure 5(c), the residual energy along the heart boundaries and aliasing artifacts along phase encoding direction were mostly suppressed. To quantify the improvement, the frame-by-frame normalized MSE plots are calculated and illustrated in Figure 6. The normalized MSE is defined by

$$\text{normalized MSE} = \frac{\|\boldsymbol{\rho} - \boldsymbol{\rho}_{True}\|_2^2}{\|\boldsymbol{\rho}_{True}\|_2^2} \quad (32)$$

where  $\|\cdot\|_2$  denotes the  $L_2$  norm and  $\boldsymbol{\rho}$  and  $\boldsymbol{\rho}_{True}$  represent the estimated- and the true  $(x, f)$  images, respectively. Clearly, more iterations consistently reduce the MSE for all frames, and the *k-t* FOCUSS results outperform that of sliding window method with the window size of four.

Our *k-t* FOCUSS algorithm has been also applied for a higher acceleration factor. As shown in Figure 7(a), excellent reconstruction quality was observed with 8-fold acceleration. However, for 16x acceleration, we started to see reconstruction artifacts over all the images (see Figure 7(c)). However, these artifacts are efficiently suppressed using parallel coils (see Figures 7(b)(d), respectively). In order to quantify these artifacts, we have also plotted an MSE for each time frame in Figure 8. As expected, more iterations result in reconstruction quality improvements, and parallel coils reduce the reconstruction errors.

For comparison, we have also illustrated the conventional *k-t* BLAST results with a *lattice sampling pattern* in Figures 9(a) and (b). Clearly, at the same acceleration factor, the wrap-around aliasing artifacts are observed in *k-t* BLAST reconstruction using a lattice sampling pattern. Of course, with the careful design of a lattice sampling pattern and sequence timing, the aliasing artifact in the *k-t* BLAST could be removed [16, 18]. However, our *k-t* FOCUSS is robust to sequence timing and *does not* need the careful design of a sampling pattern thanks to the power of the random sampling scheme.

## 4.2. fMRI Experiments

*4.2.1. Methods* The fMRI (functional MRI) is a technique that monitors brain hemodynamics. When a person is thinking or doing something, the nerve cells of his/her brain are activated by consuming oxygen in the blood. This phenomenon results in changes in the magnetic state of hemoglobin. As a consequence, we can detect a slightly different magnetic resonance signal of blood in the brain.

For fMRI study, we designed a right finger tapping experiment using a block paradigm. The goal of this experiment was to figure out which part of brain is activated when the right finger moves. We asked a subject to tap the right finger when a “tap” sign appeared, and stop tapping when a “stop” sign was presented. These tasks were periodically performed ten times. Each right finger tapping task was performed during 21 seconds, and the resting period between successive right finger tapping tasks was 30 seconds. Informed consent was obtained from each volunteer. *In vivo* brain data were acquired using a 3.0T MRI system manufactured by ISOL technology of Korea. A birdcage RF head coil was used for both the RF pulse transmission and the signal detection. We have acquired 184 frames with 3 sec TR. The first 14 frames were obtained for calibration. From the 15th frame, every 17 frames show one block of the right finger tapping experiments. The acquisition sequence was EPI with a flip angle of 80 degrees. We have obtained k-space data on a  $64 \times 64$  matrix size. The number of slices was 35, and the thickness of each slice was 4mm. Each voxel size was  $3.4375 \times 3.4375 \times 4 \text{ mm}^3$ , so we could obtain a  $220 \times 220 \text{ mm}^2$  Field Of View (FOV). After we obtained the full k-space data, we used the SPM (statistical parametric mapping [32]) toolbox on Matlab to analyze the activated parts during the right finger tapping. From the full k-space data, we applied random downsampling to obtain partial k-space data. The sampling pattern was similar to Figure 1. Since the downsampled data was obtained directly from the complex valued k-space data, no Hermitian symmetry was assumed. By applying our k-t FOCUSS algorithm for each slice, we reconstructed aliasing free 3-D brain image sequences. Here, we used a slightly different temporal transform method from the *in vivo* cardiac cine imaging experiment. As shown in Figure 10 (a), the original x-f support obtained from fully sampled data was spread over whole frequency, so we applied the KLT/PCA to make the signal much sparser. The principal components were calculated from low resolution x-f support obtained using only low frequency k-space samples. As shown in Figure 10 (b), the KLT/PCA significantly reduces the non-zero coefficients. To calculate the activated area and compare it with the reference model, SPM toolbox was again used with exactly the same parameters as in the full data case for the reconstructed sequences.

*4.2.2. Results* We have applied our k-t FOCUSS algorithm for the reduction factors of 8. A total of five k-t FOCUSS iterations were applied. Then, we used the SPM toolbox to analyze the activated area using the final k-t FOCUSS reconstruction results. In fact, the SPM detection of the activated area is calculated from the slight differences of the time varying images. Even if we have already verified our algorithm using the cardiac cine, the

main goal of the fMRI experiment is to additionally confirm that our *k-t* FOCUSS can catch even the slight differences hardly visible with the naked eye.

The reference and *k-t* FOCUSS reconstruction with 8x downsampling are shown in Figures 11(a), and (b), respectively. Visually similar results were obtained. Now, we use the SPM toolbox to calculate the activated area, as shown in Figures 12(b) for reduction factors 8. The result in Figure 12 (a) illustrates the activated detection part from the full *k*-space data, which confirms the fact that the left motor cortex is activated during right finger tapping. We used this result as a reference model to verify the performance of our algorithm for an fMRI study. We overlaid the activated area to the brain phantom, as shown in the right column of Figure 12, using the SPM toolbox. The *p*-values for SPM analysis was 0.05 for all the experiments. Figure 12(b) illustrates the reconstruction results using our *k-t* FOCUSS at the 8-fold downsampling factor. Compared to the results obtained from the fully sampled data, the activated areas in Figure 12(b) are somewhat weaker, but the strongly activated parts are still correctly identified. Additionally, we also plotted the average time curve for the activated area in Figure 13. We can see that the *k-t* FOCUSS results follow that of the full data reference, as illustrated in Figure 13. To confirm the performance improvement of *k-t* FOCUSS over conventional processing, we generated the reconstruction results using only the eight lowest *k*-space frequency samples (i.e. 8-fold acceleration) in Figure 12 (c), which clearly shows the blurred map of the activated area and even indicates the activation outside of the brain. Furthermore, by comparing Figure 11 (b) and (c), we clearly see that our *k-t* FOCUSS algorithm shows very clear reconstruction results, even from very limited data samples.

So far, small EPI matrix sizes were unavoidable for fMRI analysis to keep the temporal resolution and to obtain time varying images without aliasing. As shown in Figures 11 (a),(b), and (c), the reconstructed image size is usually  $64 \times 64$ . Since this size is too small to show the accurate coordinate of the activated area on the brain, we need to up-sample the reconstructed images to a much larger size. To map the small size image to a larger size, a T1 image is used as a large reference brain image, as shown in Figure 11 (d). In our experiment, a T1 image of  $256 \times 256$  size was acquired before the right finger tapping task. As a consequence, artifacts are unavoidable during the registration with the high resolution T1 images. However, the *k-t* FOCUSS algorithm could allow a larger image size during the same  $T_R$  without aliasing artifacts. Hence, we expect that *k-t* FOCUSS might be a valuable tool for high resolution fMRI.

## 5. Discussion

### 5.1. Hyper Parameter Setting

There are multiple hyper parameters that affect the performance of the *k-t* FOCUSS, such as the regularization factor  $\lambda$  in Eq. (17), the power factor  $p$  in Eq. (15), and the number of iterations. The parameter  $\lambda$  controls the stability of the solution under noisy conditions.

Figure 14 shows the reconstruction results from *k-t* samples from a low signal-to-noise ratio (SNR) body coil with various  $\lambda$ . For a small  $\lambda$ , the *k-t* FOCUSS reconstruction results become noisier. On the other hand, for an appropriately large  $\lambda$ , the noise pattern disappears while the reconstruction becomes slightly smoothed out. For most of the high quality *k-t* measurements from a real scanner, we found that  $\lambda = 0.1$  performs best.

Figure 15(a)-(b) illustrate the effects of the power factor  $p$ . If  $p$  approaches 1, the solution becomes more sparse and only strong frequency features are reconstructed, resulting in visually annoying artifacts, as shown in Figure 15(a). Figure 15(b) is the reconstruction results with  $p = 0.5$ , which is the best in reconstruction quality.

### 5.2. Lattice Sampling Pattern

Similar to a *k-t* BLAST using a lattice sampling pattern, the computational complexity of *k-t* FOCUSS could be greatly reduced if the  $(k, t)$  samples were obtained on the lattice. More specifically, let us define a 2-dimensional lattice  $\Lambda$  as

$$\Lambda = \{n_1 \mathbf{v}_1 + n_2 \mathbf{v}_2 : n_1, n_2 \in \mathbb{Z}\} \quad (33)$$

where  $\mathbf{v}_1$  and  $\mathbf{v}_2$  are linearly independent vectors and  $n_1, n_2$  are integers. Here,  $\mathbf{V} = [\mathbf{v}_1, \mathbf{v}_2]$  denotes the sampling matrix or basis matrix, and the sampling density is defined by  $1/d(\mathbf{V})$ , where  $d(\mathbf{V})$  denotes the determinant of matrix  $\mathbf{V}$ . The reciprocal lattice  $\Lambda^*$  is then defined as the lattice that has the basis matrix  $\mathbf{V}^* = \mathbf{V}^{-T}$ , where  $\mathbf{V}^{-T}$  denotes the transpose of the inverse of  $\mathbf{V}$ .

Suppose that the continuous signal  $v(k, t)$  is sampled on lattice  $\Lambda$ . Then, the corresponding 2-D Fourier transform  $\theta(x, f)$  of the sampled  $v(k, t)$  is composed of replicas on the reciprocal lattice  $\Lambda^*$  [33]:

$$\theta \left( \begin{bmatrix} x \\ f \end{bmatrix} \right) = \frac{1}{d(\mathbf{V})} \sum_{n_1, n_2} \rho \left( \begin{bmatrix} x \\ f \end{bmatrix} - \mathbf{V}^{-T} \begin{bmatrix} n_1 \\ n_2 \end{bmatrix} \right). \quad (34)$$

In operator form, Eq. (34) can be written as

$$\boldsymbol{\theta} = \mathbf{M}\boldsymbol{\rho} \quad (35)$$

where  $\mathbf{M}$  denotes the overlap index operator, whose  $(i, j)$  elements are 1 if contribution exists from the  $j$ -th original  $(x, f)$ -pixel to the  $i$ -th *aliased*  $(x, f)$  pixel; otherwise it is zero. Then, our *k-t* FOCUSS update equation for Eq. (35) can be simplified by

$$\boldsymbol{\rho}_n = \boldsymbol{\Theta}_n \mathbf{M}^H (\mathbf{M} \boldsymbol{\Theta}_n \mathbf{M}^H + \lambda \mathbf{I})^{-1} \boldsymbol{\theta} \quad (36)$$

or in another offset form:

$$\boldsymbol{\rho}_n = \bar{\boldsymbol{\rho}} + \boldsymbol{\Theta}_n \mathbf{M}^H (\mathbf{M} \boldsymbol{\Theta}_n \mathbf{M}^H + \lambda \mathbf{I})^{-1} (\boldsymbol{\theta} - \mathbf{M} \bar{\boldsymbol{\rho}}). \quad (37)$$

Due to the special structure of the overlap index matrix  $\mathbf{M}$ , Eqs. (36) and (37) can be decomposed into a pixel by pixel update in the  $(x, f)$  space [16].

However, the main weakness of such a modification of k-t FOCUSS is that the lattice sampling pattern does not satisfy the assumption for the compressed sensing theory [20]. Hence, we can easily expect that the advantage of the k-t FOCUSS over k-t BLAST/SENSE should not be significant in the lattice sampling pattern compared to the random sampling pattern.

### 5.3. Computational Complexity

As discussed above, k-t FOCUSS is more effective for a random sampling pattern rather than a lattice sampling pattern. However, for the random sampling pattern, the main drawback of k-t FOCUSS is the computational burden. Note that the computational burden for the k-t FOCUSS comes from the matrix inverse in Eqs. (16) and (17).

In order to reduce the computational burden of k-t FOCUSS, the matrix inversion is skipped by using a conjugate gradient (CG) method [34]. In CG, the most important step is the calculation of the gradient. The gradient of the cost function Eq. (12) with respect to  $\mathbf{q}$  is given by

$$\frac{\partial C(\mathbf{q})}{\partial \mathbf{q}} = -\mathbf{W}_n^H \mathbf{F}^H (\mathbf{v} - \mathbf{F}\bar{\rho} - \mathbf{F}\mathbf{W}\boldsymbol{\rho}) + \lambda \mathbf{q} \quad (38)$$

which can be decomposed into the following consecutive steps:

$$\text{Weighting:} \quad \mathbf{W}\mathbf{q} \quad (39)$$

$$\text{2-D Fourier transform:} \quad \mathbf{F}\mathbf{W}\mathbf{q} \quad (40)$$

$$\text{Substraction:} \quad \mathbf{v} - \mathbf{F}\bar{\rho} - \mathbf{F}\mathbf{W}\mathbf{q} \quad (41)$$

$$\text{2-D inverse Fourier transform:} \quad \mathbf{F}^H (\mathbf{v} - \mathbf{F}\bar{\rho} - \mathbf{F}\mathbf{W}\mathbf{q}) \quad (42)$$

$$\text{Weighting and Sum:} \quad -\mathbf{W}^H \mathbf{F}^H (\mathbf{v} - \mathbf{F}\bar{\rho} - \mathbf{F}\mathbf{W}\mathbf{q}) + \lambda \mathbf{q} \quad (43)$$

since the inverse Fourier transform is the adjoint of the fast Fourier transform. The main computational burden comes from Eqs. (40) and (42). The fast Fourier transform (FFT), however, may significantly relieve the computational burden of these steps. In our *in vivo* cardiac experiment, the total 3D matrix size to be reconstructed was  $220 \times 256 \times 25$ . Using Matlab 7.0.4 on Xeon 3GHz with 2 GB RAM, it took 100 sec to reconstruct the final cardiac cine using our k-t FOCUSS algorithm with five iterations.

## 6. Conclusion

Using a random k-t sampling pattern and FOCUSS algorithm, we designed a new dynamic imaging algorithm called k-t FOCUSS, which is asymptotically optimal from the compressed sensing theory and encompasses the celebrated k-t BLAST and k-t SENSE as special cases. Our k-t FOCUSS does not require a training phase or *a priori* knowledge of x-f support. Furthermore, thanks to the random sampling pattern, our k-t FOCUSS is robust and insensitive to the sequence timing. We have applied our k-t FOCUSS to dynamic MR

imaging problems, such as cardiac cine and fMRI experiments and obtained highly improved reconstruction from severely downsampled *k*-space data.

Despite the surprising performance of *k-t* BLAST and *k-t* SENSE, a theoretical explanation for their algorithm was not sufficient. Our analysis showed that *k-t* BLAST/SENSE is indeed the first iteration of our *k-t* FOCUSS algorithm and the diagonal covariance matrix in *k-t* BLAST/SENSE is actually the reweighted matrix updated from the initial low resolution estimate. We expect that the insight we have acquired from the development of *k-t* FOCUSS not only improves the quality of the *k-t* BLAST and *k-t* SENSE, but also opens a new area of research.

## 7. Acknowledgements

This research was supported in part by a Brain Neuroinformatics Research program by Korean Ministry of Commerce, Industry, and Energy, and in part by grant No. 2004-020-12 from the Korea Ministry of Science and Technology (MOST). The authors would like to thank Dr. Byung Wook Choi at Yonsei Medical Center for various discussions.

## References

- [1] M. K. Stehling, R. Turner, and P. Mansfield, "Echo-planar imaging: magnetic resonance imaging in a fraction of a second," *Science*, vol. 254, no. 5028, pp. 43–50, October 1991.
- [2] H. Y. Carr, "Steady-state free precession in nuclear magnetic resonance," *Phys. Rev.*, vol. 112, no. 5, pp. 1693–1701, December 1958.
- [3] S. Plein, T. N. Bloomer, J. P. Ridgway, T. R. Jones, G. J. Bainbridge, and M. U. Sivananthan, "Steady-state free precession magnetic resonance imaging of the heart: Comparison with segmented *k*-space gradient-echo imaging," *J. Magnetic Resonance Imaging*, vol. 14, no. 3, pp. 230–236, 2001.
- [4] V. S. Lee, *Cardiovascular MRI: Physical Principles to Practical Protocols*, Lippincott Williams & Wilkins, 2005.
- [5] D. K. Sodickwon and W. J. Manning, "Simultaneous acquisition of spatial harmonics(SMASH): fast imaging with radiofrequency coil arrays," *Magn. Reson. Med*, vol. 38, no. 4, pp. 591–603, October 1997.
- [6] K. P. Pruessmann, M. Weigher, M. B. Scheidegger, and P. Boesiger, "SENSE: Sensitivity encoding for fast MRI," *Magn. Reson. Med*, vol. 42, no. 5, pp. 952–962, 1999.
- [7] M. A. Griswold, P. M. Jakob, M. Nittka, J. W. Goldfarb, and A. Haase, "Partially parallel imaging with localized sensitivities(PILS)," *Magn. Reson. Med*, vol. 44, no. 4, pp. 602–609, 2000.
- [8] M. A. Griswold, P. M. Jakob, R. M. Heidemann, M. Nittka, V. Jellus, J. Wang, B. Kiefer, and A. Haase, "Generalized autocalibrating partially parallel acquisitions(GRAPPA)," *Magn. Reson. Med*, vol. 47, no. 6, pp. 1202–1210, 2002.
- [9] B. Madore, G. H. Glover, and N. J. Pelc, "Unaliasing by Fourier-encoding the overlaps using the temporal dimension(UNFOLD), applied to cardiac imaging and fMRI," *Magn. Reson. Med*, vol. 42, no. 5, pp. 813–828, 1999.
- [10] Nitin Aggarwal, Qi Zhao, and Yoram Bresler, "Spatio-temporal modeling and minimum redundancy adaptive acquisition in dynamic MRI," in *Proc. 1st IEEE Int.Symp. Biomed. Imag. ISBI-2002*, July 2002, pp. 737–740.
- [11] N.P. Willis and Y. Bresler, "Optimal scan for time-varying tomography II: Efficient design and experimental validation," *IEEE Trans. on Image Processing*, vol. 4, no. 5, pp. 654–666, May 1995.

- [12] Peter Kellman, Frederick H. Epstein, and Elliot R. McVeigh, “Adaptive sensitivity encoding incorporating temporal filtering (TSENSE),” *Magn. Reson. Med.*, vol. 45, no. 5, pp. 846 – 852, 2001.
- [13] J. Tsao, “On the UNFOLD method,” *Magn. Reson. Med.*, vol. 47, no. 1, pp. 202–207, 2002.
- [14] Behzad Sharif and Yoram Bresler, “Optimal multi-channel time-sequential acquisition in dynamic MRI with parallel coils,” in *Proc. IEEE Int.Symp. Biomed. Imag. ISBI-2006*, May 2006.
- [15] Jinhee Kim, Jong Chul Ye, and Jaeheung Yoo, “x-f SENSE: Optimal spatio-temporal sensitivity encoding for dynamic MR imaging,” in *Proc. IEEE Int. Symp. Biomed. Imag. ISBI-2006*, Arlington, Virginia, April 2006.
- [16] Jeffrey Tsao, P. Boesiger, and K. P. Pruessmann, “k-t BLAST and k-t SENSE: Dynamic MRI with high frame rate exploiting spatiotemporal correlations,” *Magnetic Resonance in Medicine*, vol. 50, no. 5, pp. 1031–1042, October 2003.
- [17] S. Kozerke, J. Tsao, Reza Razavi, and P. Boesiger, “Accelerating cardiac cine 3D imaging using k-t BLAST,” *Magn. Reson. Med.*, vol. 52, pp. 19–26, 2004.
- [18] J. Tsao, S. Kozerke, P. Boesiger, and K. P. Pruessmann, “Optimizing spatiotemporal sampling for k-t BLAST and k-t SENSE: Application to high-resolution real-time cardiac steady-state free precession,” *Magn. Reson. Med.*, vol. 53, pp. 1372–1382, 2005.
- [19] M. S. Hansen, S. Kozerke, K. P. Pruessman, P. Boesiger, E. M. Pedersen, and J. Tsao, “One the influence of training data quality in k-t BLAST reconstruction,” *Magn. Reson. Med.*, vol. 52, pp. 1175–1183, 2004.
- [20] D. L. Donoho, “Compressed sensing,” *IEEE Trans. on Information Theory*, vol. 52, no. 4, pp. 1289–1306, April 2006.
- [21] E. Candes, J. Romberg, and T. Tao, “Robust uncertainty principles: Exact signal reconstruction from highly incomplete frequency information,” *IEEE Trans. on Info. Theory*, vol. 52, no. 2, pp. 489–509, Feb. 2006.
- [22] M. Lustig, J.M. Santos, D.L. Donoho, and J.M Pauly, “k-t SPARSE: High frame rate dynamic MRI exploiting spatio-temporal sparsity,” in *Proceedings of ISMRM*, Seattle, WA, April 2006.
- [23] M. Lustig, , D.L. Donoho, and J.M Pauly, “Rapid MR imaging with compressed sensing and randomly under-sampled 3DFT trajectories,” in *Proceedings of ISMRM*, Seattle, WA, April 2006.
- [24] O. Portniaguine, C. Bonifasi, E. DiBella and R. Whitaker, “Inverse methods for reduced k-space acquisition,” in *Proceedings of ISMRM*, p.481, Toronto, Canada; 2003
- [25] I. F. Gorodnitsky, J. S. George, and B. D. Rao, “Neuromagnetic source imaging with FOCUSS: a recursive weighted minimum norm algorithm,” *Electroencephalogr Clin Neurophysiol.*, vol. 95, no. 4, pp. 231–51, October 1995.
- [26] I. F. Gorodnitsky and B. D. Rao, “Sparse signal reconstruction from limited data using FOCUSS: re-weighted minimum norm algorithm,” *IEEE Trans. on Signal Processing*, vol. 45, no. 3, pp. 600–616, March 1997.
- [27] K. Kreutz-Delgado, J. F. Murray, B. D. Rao, K. Engan, T. W. Lee, and T. J. Sejnowski, “Dictionary learning algorithms for sparse representation,” *Neural Computation*, vol. 15, no. 2, pp. 349–396, 2003.
- [28] E. Candes, J. Romberg, and T. Tao, “Stable signal recovery from incomplete and inaccurate measurements,” *Communications on Pure and Applied Mathematics*, vol. 59, no. 8, pp. 1207–1233, August 2006.
- [29] J. Haupt and R. Nowak, “Signal reconstruction from noisy random projections,” *IEEE Trans. on Info. Theory*, vol. 52, no. 9, pp. 4036–4048, Sept. 2006.
- [30] E. Candes and T. Tao, “Decoding by linear programming,” *IEEE Trans. on Info. Theory*, vol. 51, no. 12, pp. 4203–4215, Dec. 2005.
- [31] H. V. Poor, *An Introduction of Signal Detection and Estimation*, Springer-Verlag, New York, 2nd edition, 1994.
- [32] K. J. Friston, A. P. Holmes, K. J. Worsley, J.-P. Poline, C. D. Frith, and R. S. J. Frackowiak, “Statistical parametric maps in functional imaging: A general linear approach,” *Human Brain Mapping*, vol. 2,

- no. 4, pp. 189–210, October 1995.
- [33] E. Dubois, “Sampling and reconstruction of time-varying imagery with application in video systems,” *Proc. of the IEEE*, vol. 73, no. 4, pp. 502–522, 1985.
- [34] E. K. P. Chong and S. H. Zak, *An Introduction to Optimization*, Wiley-Interscience, New York, 1996.

Figure Caption

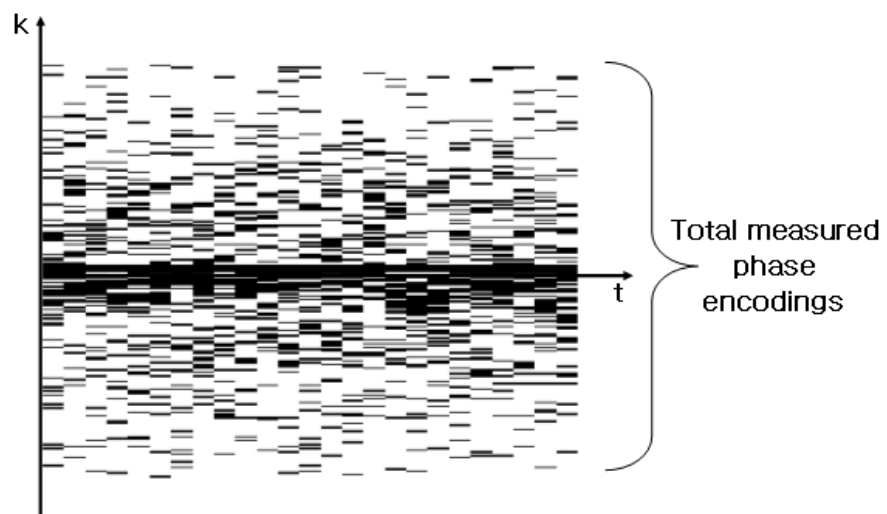
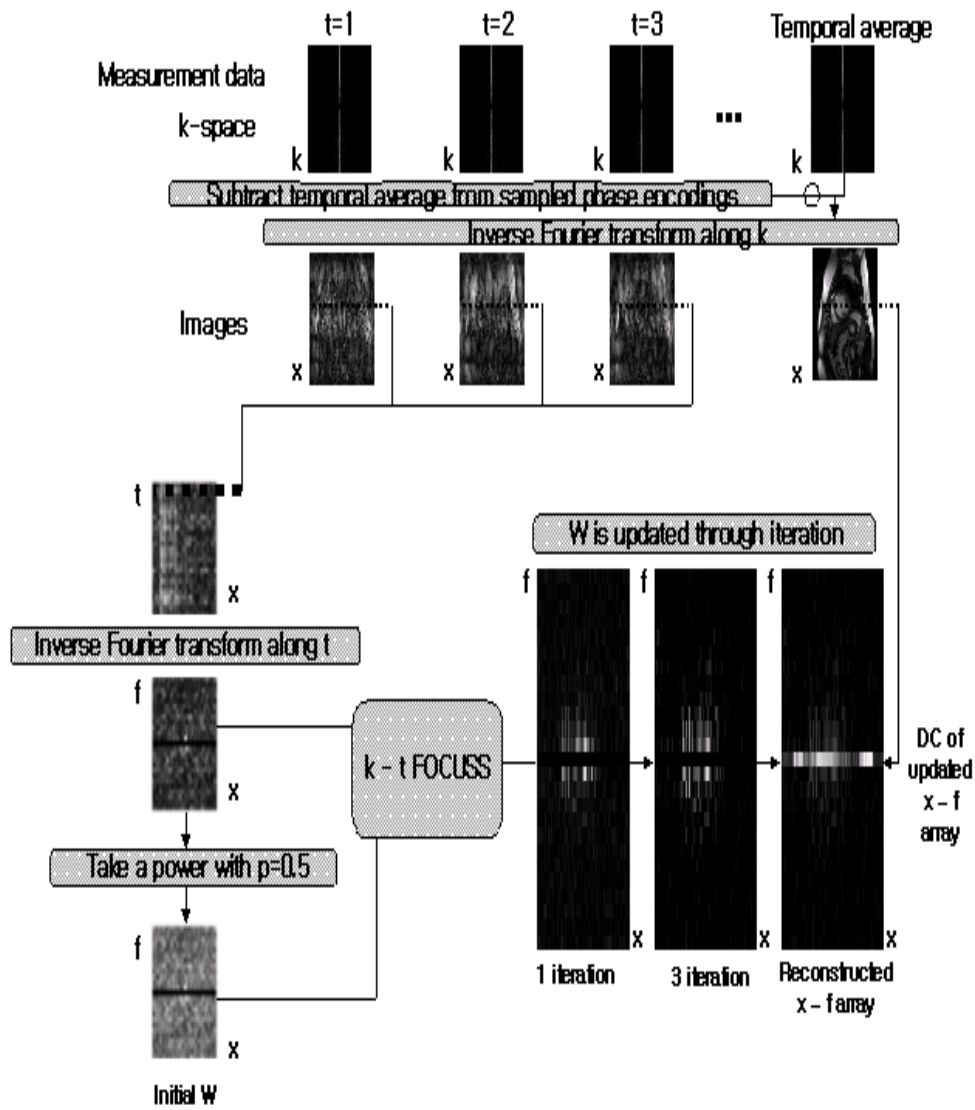
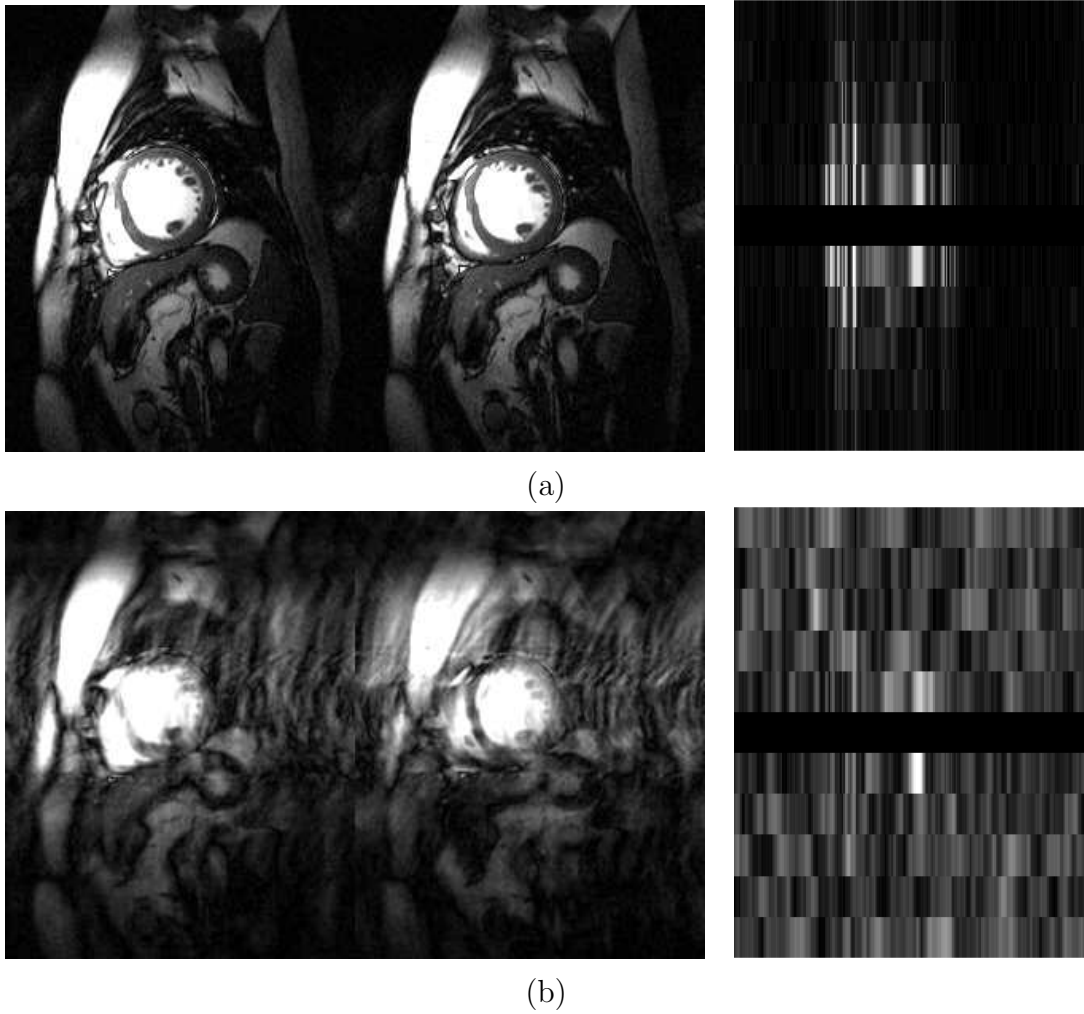


Figure 1. Gaussian random sampling pattern.



**Figure 2.**  $k$ - $t$  FOCUSS reconstruction flow. In  $k$ - $t$  FOCUSS, an estimate of the  $(x, f)$  support is updated with iterations.



**Figure 3.** *In vivo* cardiac cine reconstructed from (a) full  $k$ -space samples, and (b) direct Fourier transform of zero padded measurement data. The right most column corresponds to the corresponding  $x$ - $f$  supports. The acceleration factor for (b) is four.

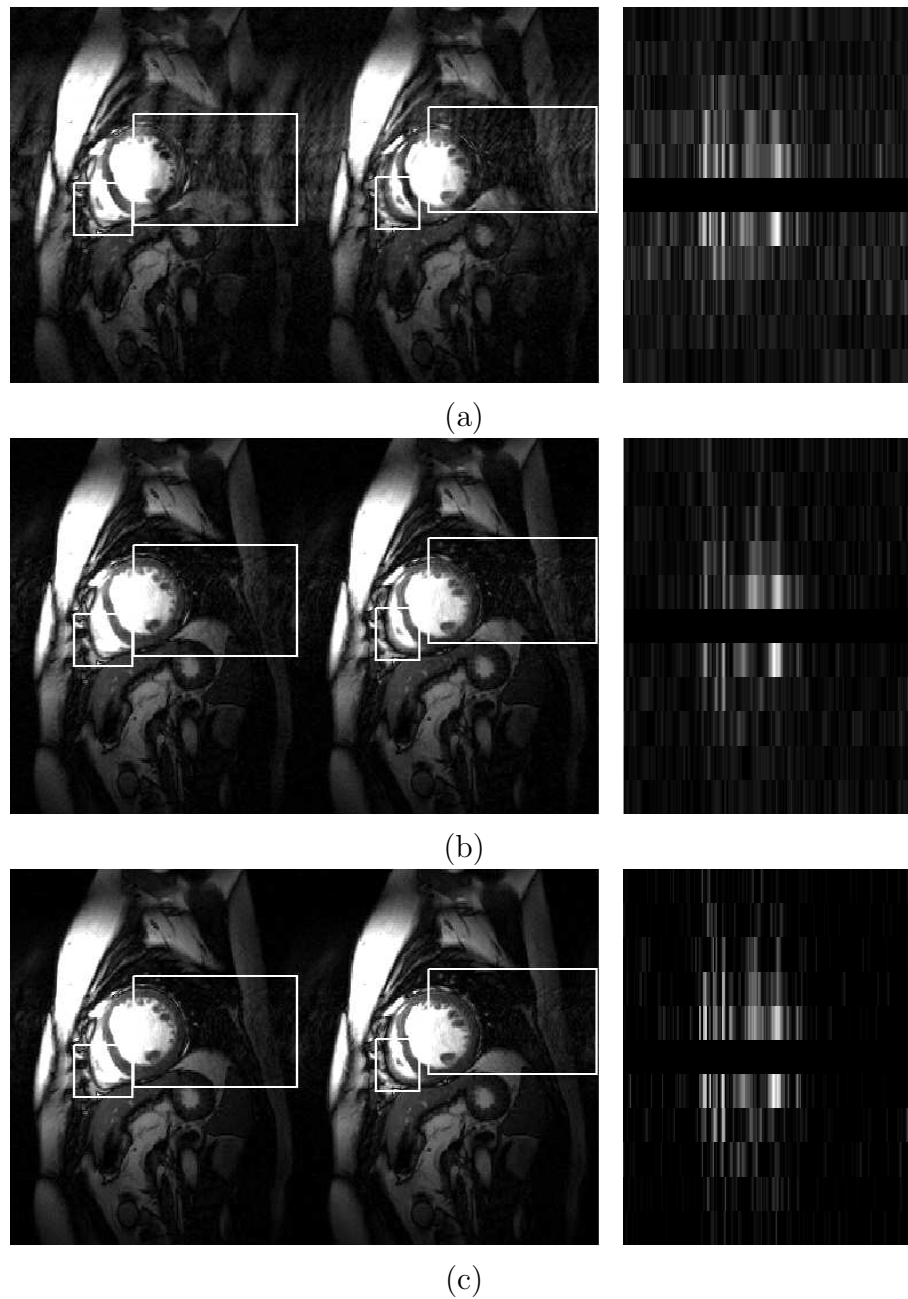
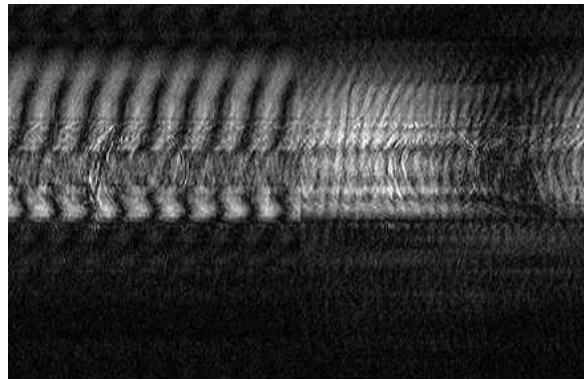
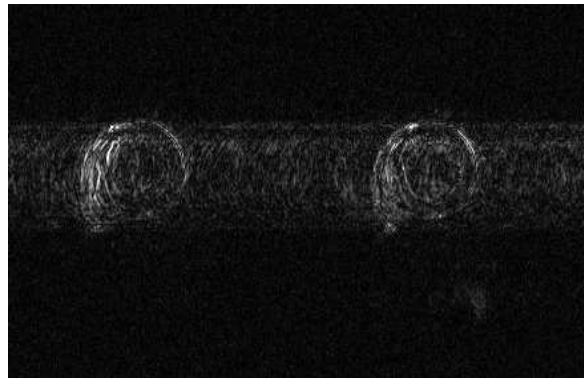


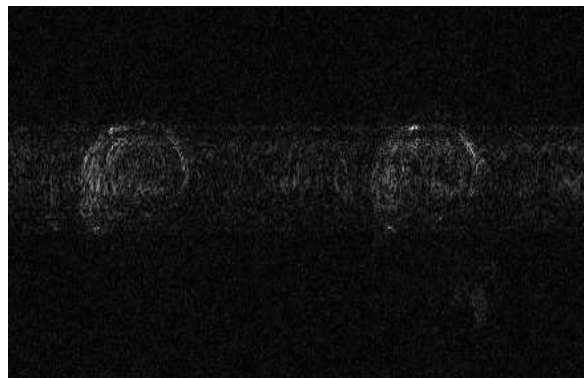
**Figure 4.** *In vivo* cardiac cine reconstructed from (a) sliding window method with the window size of 4, (b)  $k$ - $t$  FOCUSS with one iteration, and (c)  $k$ - $t$  FOCUSS with five iterations, respectively. The highly improved parts are highlighted by white boxes. The right most column corresponds to the corresponding  $x$ - $f$  supports. The acceleration factor is four.



(a)



(b)



(c)

**Figure 5.** The difference images between the original cine images and reconstructions from (a) sliding window method with the window size of 4, (b)  $k$ - $t$  FOCUSS with one iteration, and (c)  $k$ - $t$  FOCUSS with five iterations, respectively. The acceleration factor is four.

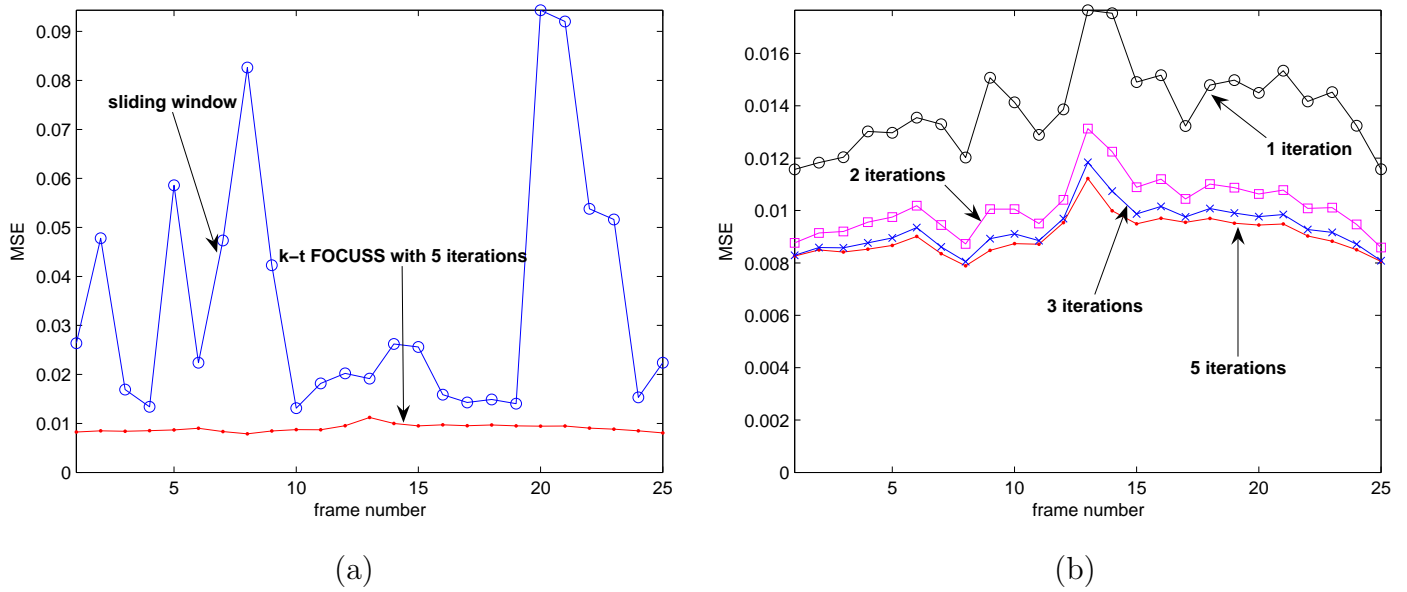


**Figure 6.** The MSE plots of  $k$ -t FOCUSS for *in vivo* cardiac data with acceleration factor of four. (a) Comparison between the sliding window and  $k$ -t FOCUSS, and (b)  $k$ -t FOCUSS results with respect to the number of iterations.

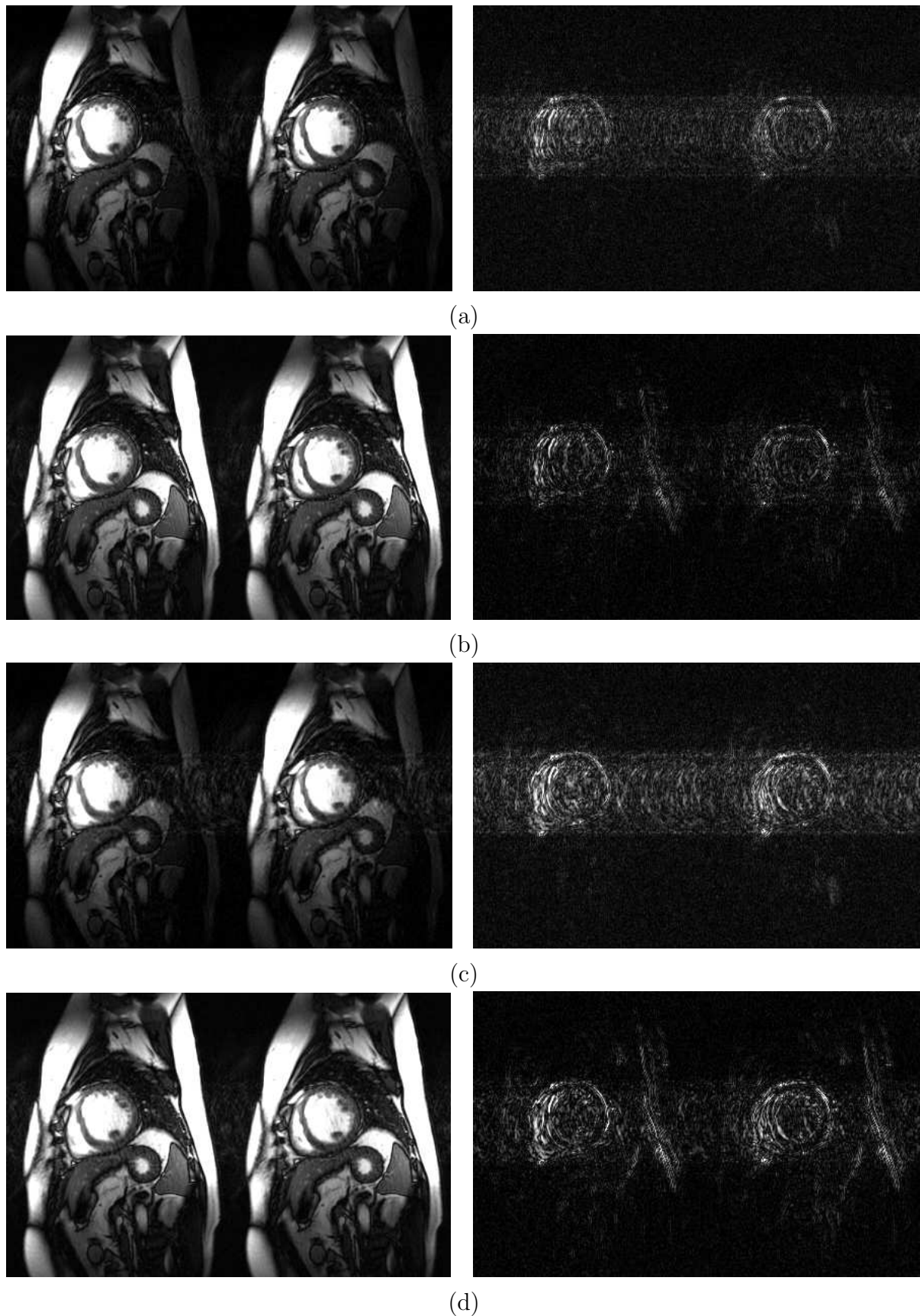


**Figure 7.** (a) Single coil  $k$ - $t$  FOCUSS reconstruction results with 8x acceleration factor; (b) Five coil parallel  $k$ - $t$  FOCUSS reconstruction with 8x acceleration factor; (c) Single coil  $k$ - $t$  FOCUSS reconstruction with 16x acceleration factor; (d) Five coil parallel  $k$ - $t$  FOCUSS reconstruction with 16x acceleration factor. Right two columns show the difference images between the original cine images and reconstructions.

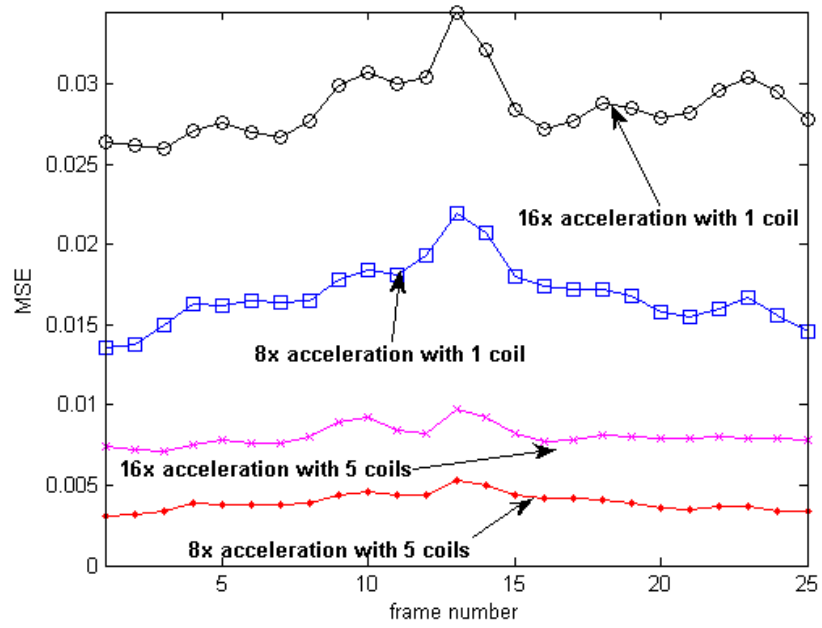


**Figure 8.** MSE plots of  $k$ - $t$  FOCUSS with 16x acceleration factor for single and 5 coils, and with 8x acceleration factor for single and 5 coils, respectively.

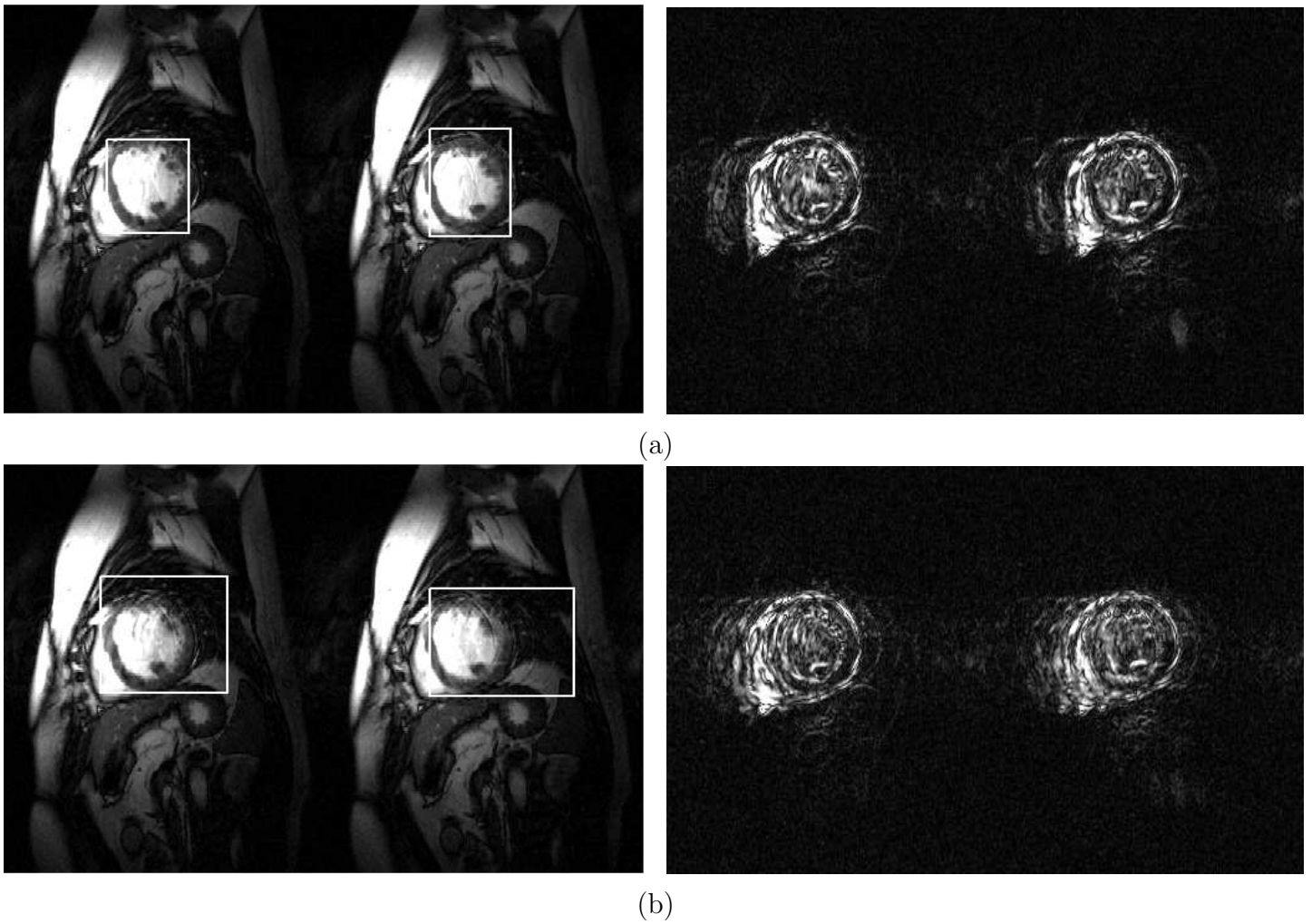
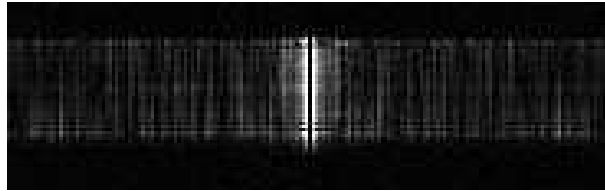
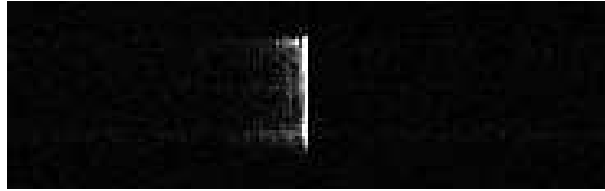


**Figure 9.**  $k$ - $t$  BLAST for lattice sampling pattern from (a) 8-fold acceleration and (b) 16-fold acceleration. The aliasing artifacts are highlighted by white boxes. Right two columns show the difference images between the original cine images and reconstructions.



(a)



(b)

**Figure 10.** (a) x-f support obtained from fully sampled data; and (b) sparse signal support after the KL transform.

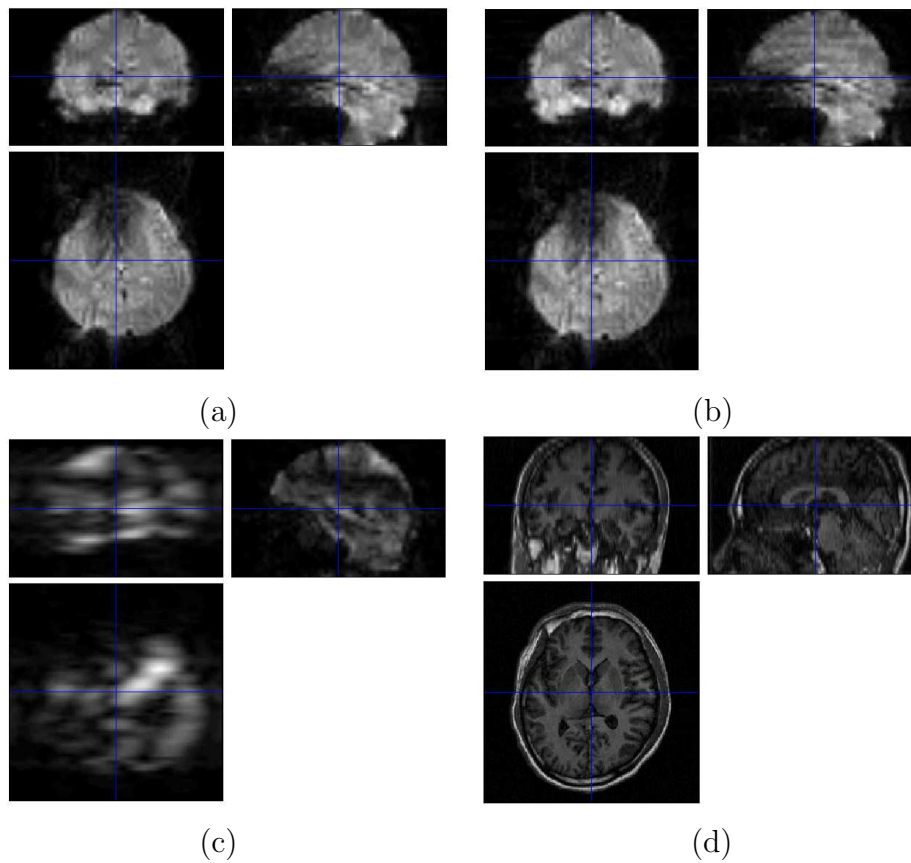


**Figure 11.** Reconstructed volumes using (a) fully sampled k-space data, (b) k-t FOCUSS at the 8-fold acceleration, and (c) low frequency only data at the 8-fold acceleration, respectively. The image size for each slice is  $64 \times 64$ . Figure (d) shows T1 image of  $256 \times 256$  size.

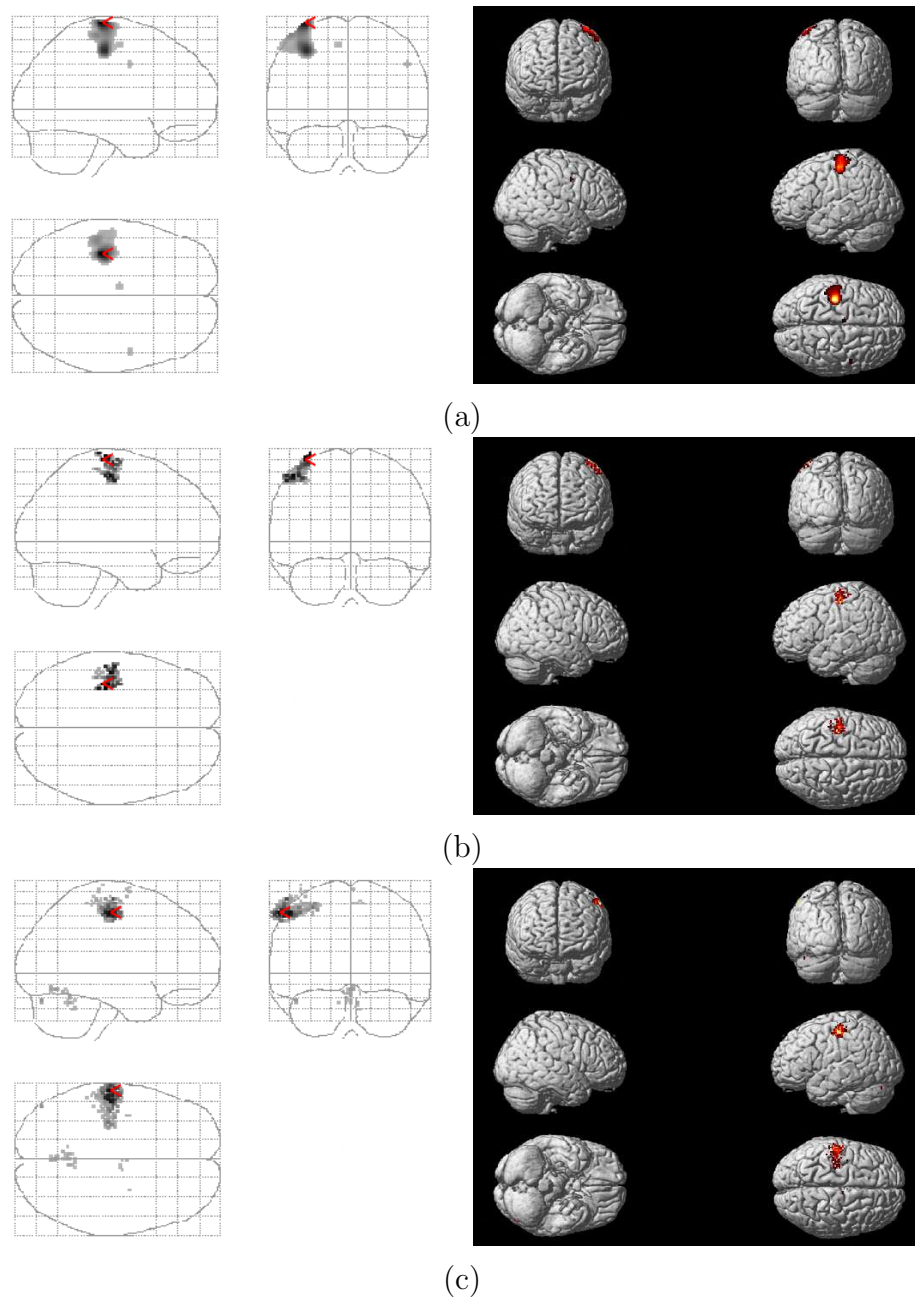


**Figure 12.** The fMRI results for right finger tapping experiment. The activated areas are calculated using the SPM toolbox from the reconstruction results using (a) original fully sampled data, (b)  $k$ - $t$  FOCUSS reconstruction at the 8-fold acceleration, and (c) low frequency data at the 8-fold acceleration, respectively.

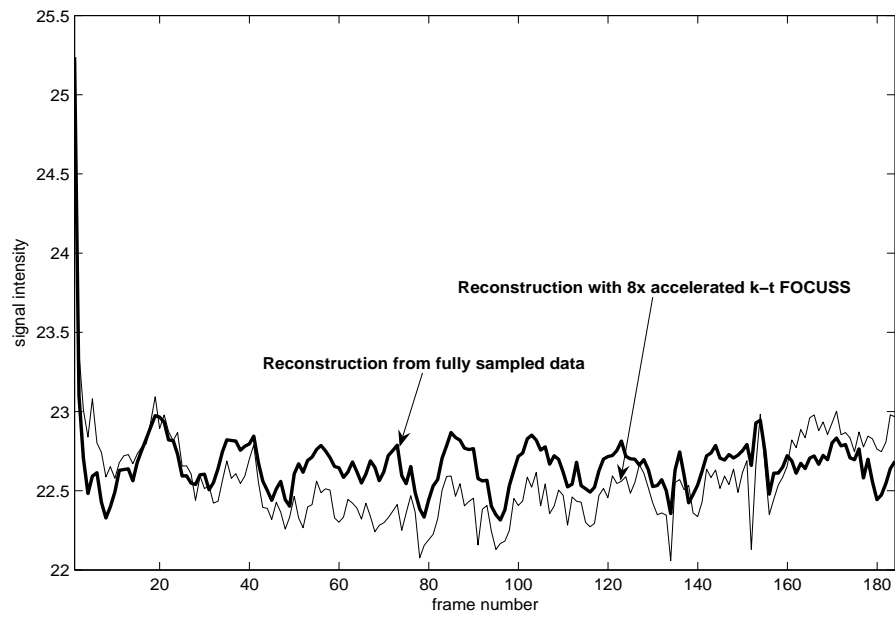
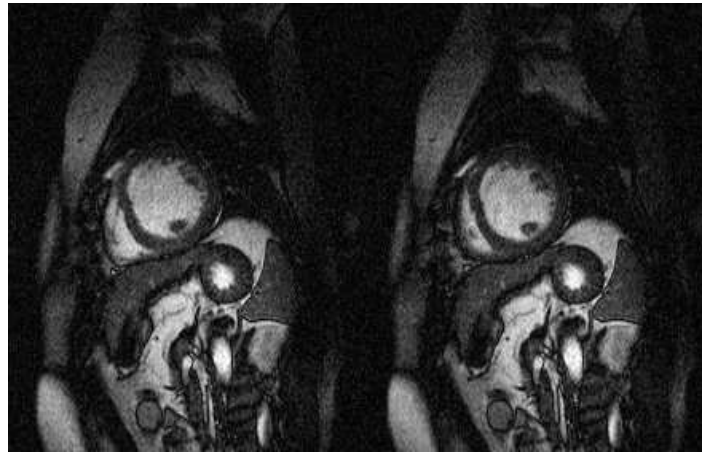
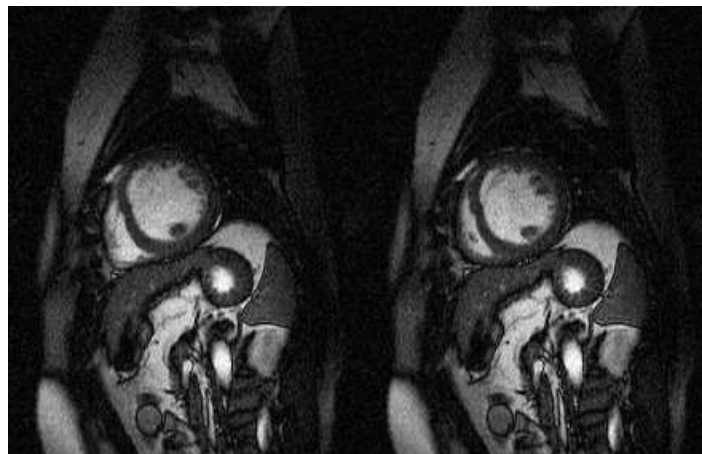


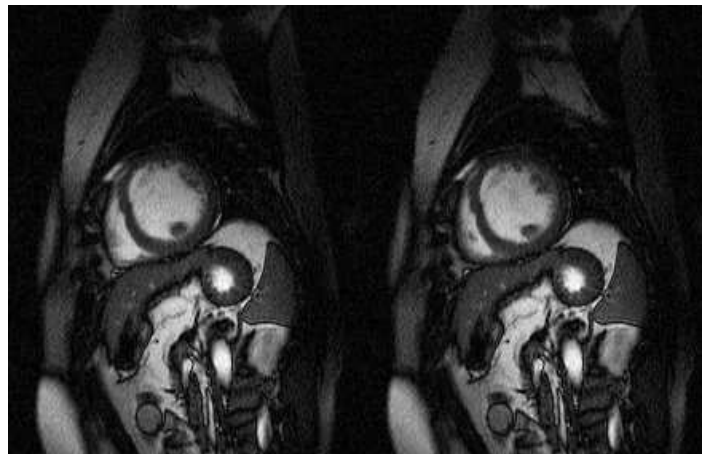
**Figure 13.** Time curve for the right finger tapping experiments



(a)

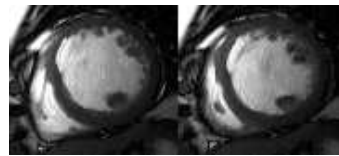


(b)

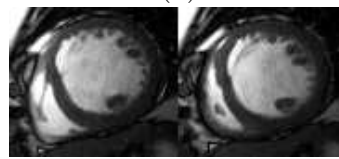


(c)

**Figure 14.**  $k$ - $t$  FOCUSS reconstruction for 4x reduction from noisy measurements with (a)  $\lambda = 0$ , (b)  $\lambda = 100$ , and (c)  $\lambda = 500$  respectively. These results are obtained after 5 iterations.



(a)



(b)

**Figure 15.**  $k$ - $t$  FOCUSS reconstruction for 4x reduction with (a)  $p = 1$ , and (b)  $p = 0.5$ . These results are obtained after 5 iterations.